Applied Catalysis B: Environmental 221 (2018) 223–234

Contents lists available at ScienceDirect

Applied Catalysis B: Environmental

journal homepage: www.elsevier.com/locate/apcatb

Enhanced photocatalytic ozonation degradation of organic pollutants by ZnO modified TiO_2 nanocomposites

Tangtao Yang, Junmin Peng, Yun Zheng, Xuan He, Yidong Hou*, Ling Wu, Xianzhi Fu

State Key Laboratory of Photocatalysis on Energy and Environment, College of Chemistry, Fuzhou University, Fuzhou, 350108, PR China

ARTICLE INFO

Keywords:
TiO_2
Photocatalytic ozonation
Synergistic effect
Water purification

ABSTRACT

Advanced oxidation processes (AOPs) for wastewater treatment have attracted much attention for their efficient capability in destroying persistent and toxic organic compounds. In this study, we reported a simple impregnation-calcination method to fabricate ZnO modified TiO_2 (Zn-TiO_2) nanocomposites and employed them as catalysts for degradation of organic pollutants in water. The results show that 7at%Zn-TiO_2 exhibits much better performances of photocatalysis, catalytic ozonation and photocatalytic ozonation than pure TiO_2, which could be due to its richer surface hydroxyl groups and higher separation efficiency of photogenerated electron-hole pairs. The total organic carbon (TOC) removal efficiency of salicylic acid (SA) in UV/O_3/7at%Zn-TiO_2 is higher than the sum of those in UV/7at%Zn-TiO_2 and O_3 processes, indicative of a synergistic effect between photocatalysis and ozonation. Mechanism studies demonstrate that the active species such as H_2O_2, h^+, ·OH, $\cdot O_2^-$ and $^1O_2$ are responsible for SA degradation. Meanwhile, the intermediates of SA mineralization were identified by HPLC–MS and its mineralization pathway was proposed. Reusability test verifies a high stability of 7at%Zn-TiO_2 in the photocatalytic ozonation process, and the catalyst can be applied in a wide pH range of aqueous solution from 3.5 to 10.0. This work puts forward a new application of the easily available Zn-TiO_2 nanocomposites and might drive the advance of photocatalytic ozonation approach for water purification.

1. Introduction

In the past few decades, the advanced oxidation processes (AOPs) have been applied in the treatment of persistent organic contaminants in water [1–3]. Simplex ozonation or photocatalysis related to AOPs, has some disadvantages that restrain their efficiency in the elimination of organic pollutants. Photocatalysis is a rather slow process due to its low oxidation rate [4], while ozonation alone often leads to incomplete mineralization of organic compounds [5]. These drawbacks make the practical application of these individual technologies to economically dispose industrial wastewater undesirable. To address these problems, the introduction of catalysts and/or light irradiation to the wastewater during ozonation is imperative to boost the elimination efficiency.

The combination of photocatalysis and ozonation has been reported as a promising and eco-friendly treatment approach for organic contaminants [6,7], because this coupled technique is capable of achieving high removal efficiency and does not reproduce any secondary pollution. Ozone, as a powerful scavenger, can quickly capture the photogenerated electrons when photocatalysis and ozonation processes are conducted simultaneously. This will facilitate the transport of photoexcited charge carriers and the utilization of ozone, accordingly, producing more active species such as h^+, ·OH, $\cdot O_2^-$ and $^1O_2$, to accelerate the decomposition and mineralization of organic pollutants [8–12].

Some semiconductor materials have been reported to trigger a synergistic effect between photocatalysis and ozonation to greatly improve the oxidation efficiency of organic contaminants [13,14]. TiO_2 is an extensively used catalyst for photocatalytic ozonation of organics due to the peculiar properties, including facile fabrication, low cost, non-toxicity, high stability and good photoreactivity [15–18]. Unfortunately, there are some shortcomings in terms of using pure TiO_2 as a catalyst for photocatalytic ozonation such as the fast recombination of photoinduced electron-holes and incomplete mineralization of organics, which somewhat impedes its practical application in wastewater treatment [12,19,20]. Thus, various effective strategies have been developed to enhance the catalytic activity of TiO_2.

The coupling TiO_2 with transition metal oxide to construct composites such as ZnO/TiO_2 [21], Cu_2O/TiO_2 [22], WO_3/TiO_2 [23,24], ZrO/TiO_2 [25], and MoO_3/TiO_2 [26,27], significantly improve the photocatalytic activity as a result of the accelerated transfer of photoinduced charge carriers and more surface hydroxyl groups. It is generally regarded that the enrichment of surface hydroxyl groups of the

* Corresponding author.
E-mail address: ydhou@fzu.edu.cn (Y. Hou).

http://dx.doi.org/10.1016/j.apcatb.2017.09.025
Received 2 July 2017; Received in revised form 4 September 2017; Accepted 11 September 2017
Available online 12 September 2017

catalyst could also enhance degradation rate and mineralization efficiency of organics in ozonation process [28]. Furthermore, ZnO has been recently reported as an effective catalyst for ozonation of organic contaminants in aqueous solution [29,30]. Following this line of thinking, the modification of TiO_2 with zinc oxide is proposed to fabricate efficient catalyst for the photocatalytic ozonation process. The studies on the generation of active species and the mineralization pathway of organics degradation in this combined technology are also carried out to better understand the oxidation mechanism.

In this study, ZnO modified TiO_2 nanocomposites were prepared by a simple impregnation-calcination method. The obtained samples were characterized by XRD, BET, TEM, SEM, XPS and electrochemical measurement in detail. Salicylic acid (SA) was selected as a model contaminant to evaluate the catalytic activity, and the survey was conducted to research the influence of various reaction parameters (*e.g.* catalyst dosage, ozone concentration, inorganic ion, initial SA concentration and solution pH) on the photocatalytic ozonation performance in UV/O_3/Zn-TiO_2 process. Electron paramagnetic resonance (EPR) and conventional quenching experiments were used to investigate the produced active species for the SA degradation and mineralization. Furthermore, the intermediates generated in UV/O_3/Zn-TiO_2 process were further affirmed by HPLC–MS and thus the mineralization pathway of SA was proposed.

2. Experimental section

2.1. Materials and reagents

Commercial TiO_2 was supplied by Degussa Co., Ltd, and other reagents with analytical grade purity were obtained from Sinopharm Chemical Reagent Co., Ltd. (China). All chemicals for the photocatalytic ozonation reactions were used as received without any further purification. The deionized water was used for all synthesis and treatment. Ozone was produced by an ozone generator (Tonglin Technology 3S-A) from high purity oxygen (Fuzhou Lianzhong Industrial Gases Co., Ltd.).

2.2. Catalyst preparation

In a typical synthesis, a certain amount of commercial TiO_2 was added into 60 mL deionized water in a 100 mL beaker and followed by stirring for 0.5 h. After that, the calculated amount of zinc nitrate solution (Zn/Ti molar ratio of 0, 1%, 3%, 7% and 10%, respectively) was added into the mixed solution and agitated for 2 h. Afterwards, the resulting mixture was placed in an oil bath with stirring at 80 °C for 12 h, and the obtained solid was put into the alumina crucible. Then the crucible was annealed in a muffle furnace at 450 °C for 3 h. The resulting products were labeled as TiO_2, 1at%Zn-TiO_2, 3at%Zn-TiO_2, 7at %Zn-TiO_2 and 10at%Zn-TiO_2, separately. Additionally, 7at%Zn-TiO_2 precursor was calcined at different temperatures (300, 350, 400, 450 and 500 °C). The acquired products were marked as 7at%Zn-TiO_2-300, 7at%Zn-TiO_2-350, 7at%Zn-TiO_2-400, 7at%Zn-TiO_2-450 and 7at%Zn-TiO_2-500, respectively.

2.3. Catalyst characterization

The crystal phase of the samples was characterized by powder X-ray diffraction (XRD, Bruker D8 Advance) with Cu Kα1 radiation. The morphologies of the materials were observed by a Hitachi New Generation SU8010 field emission scanning electron microscope (FESEM). Transmission electron microscopy (TEM) images were collected by a JEOL model JEM 2010 EX instrument. X-ray photoelectron spectra (XPS) measurements were conducted on a Thermo Fisher Scientific ESCALAB 250Xi spectrometer with the C 1 s peak (284.8 eV) as a reference. The nitrogen adsorption and desorption isotherms were performed with an ASAP 2020 apparatus (Micromeritics Instrument Corp., USA) at 77 K. The Electron paramagnetic resonance (EPR) signals of radicals were detected by a Bruker model A300 spectrometer with 5, 5-dimethyl-1-pyrroline (DMPO) and 2, 2, 6, 6-tetramethy l-4-piperidinol (TEMP) as spin-trapping agents.

2.4. Photocatalysis, ozonation and photocatalytic ozonation experiments

The degradation of SA aqueous solution was performed for the evaluation of catalytic activity of the samples under ambient condition. A semibatch reactor was composed of quartz glass with the dimensions of 5 cm diameter and 18 cm tall. 150 mL of SA solution with the initial concentration of 80 ppm, unless specifically stated, was poured into the quartz reactor for the photocatalytic ozonation reactions. In a typical process, 75 mg of as-prepared catalyst was added into the SA solution and magnetically stirred in dark for 0.5 h to achieve adsorption-desorption equilibrium before reaction. The effect of pH value on the activity was studied by adjusting the pH value of solution with NaOH solution (0.1 mol/L). The reactor was surrounded by four portable UV lamps (Philips, TUV 6W G6 T5, 254 nm) as the UV light source, and the gaseous ozone was bubbled by the inlet at the bottom of the reactor with a flow rate of 30 mL/min. The photocatalytic ozonation reaction was performed under UV light irradiation and O_3 gas bubbling. At each given time interval, 4 mL of the suspension solution was taken out from the reactor and injected into a vial through a 0.22 μm microfilter to obtain the clear solution. A certain amount of $Na_2S_2O_3$ solution (0.1 mol/L) was added into the taken aqueous sample to trap the residual O_3. Single photocatalysis, catalytic ozonation, ozonation alone and photolysis (without catalyst) were also carried out under the identical conditions.

2.5. Analytical methods

The concentration of SA aqueous solution was measured by a UV–vis spectrophotometer (Varian Cary 50 Conc, USA) at a wavelength of 296 nm. Total organic carbon (TOC) of the SA solution was measured with a Shimadzu TOC-VCPH analyzer. The degradation intermediates of SA were detected by high-performance liquid chromatography-mass spectrometry (HPLC–MS, Agilent 6520, Q-TOF LC/MS) equipped with a multiple UV-detector (Agilent 1260) and a SunFire ® C18 column (5 μm, 4.6 × 150 mm). The mobile phase was made of deionized water and methanol with a flow rate of 1.0 mL/min. The injection volume was 20 μL with an autosampler. The gradient started with 60% methanol, increased to 90% within 3.0 min and equilibrated within 1.0 min, then returned to the initial composition within 1.0 min. The MS was operated in a negative mode using ESI and the parameters were set as follows: capillary voltage, 4000 V; nebulization pressure, 40 psi; temperature of drying gas, 350 °C; drying gas flow, 10.0 L/min. Full-scan spectra were acquired by *m/z* scanning from 20 to 250. To investigate the active species generated in the photocatalytic ozonation processes, the experiments of free radicals capture were carried out by adding ammonium oxalate (AO, a quencher of h^+) and *tert*-butanol (TBA, a quencher of ·OH), respectively. N, N-diethyl-*p*-phenylendiamine (DPD) method was employed for the detection of H_2O_2. The solution pH was examined with a pH-meter (Oakton Waterproof pHTestr 10).

2.6. Electrochemical measurements

The photoelectrochemical measurements were carried out in a typical three-electrode cell with 0.2 mol/L Na_2SO_4 as the electrolyte solution using a CHI 660D electrochemical workstation (Shanghai, China). The Ag/AgCl electrode and platinum sheet were regarded as a reference electrode and counter electrode, respectively. A 300 W Xe lamp was served as a simulated light source and the periodic ON/OFF photocurrent response was measured at a definite time interval. Electrochemical impedance spectroscopy (EIS) was performed by an electrochemical analyzer (Zahner, Germany). The measurements were carried out by applying an AC voltage of 10.0 mV to the electrode over

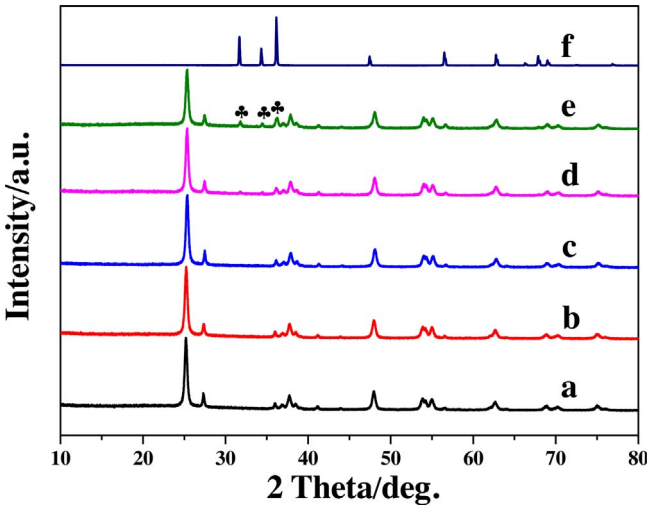

Fig. 1. XRD patterns of TiO_2 (a), Zn-TiO_2 with different Zn content, 1at% (b), 3at% (c), 7at% (d), 10at% (e) and ZnO (f).

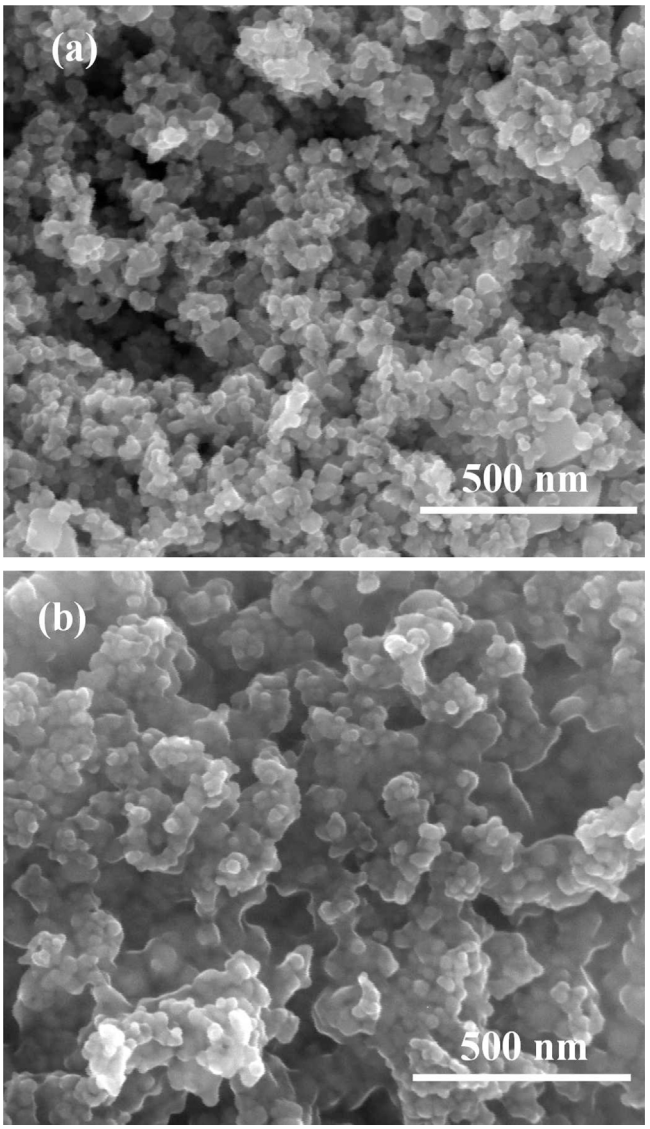

Fig. 2. SEM images of TiO_2 (a) and 7at%Zn-TiO_2 (b).

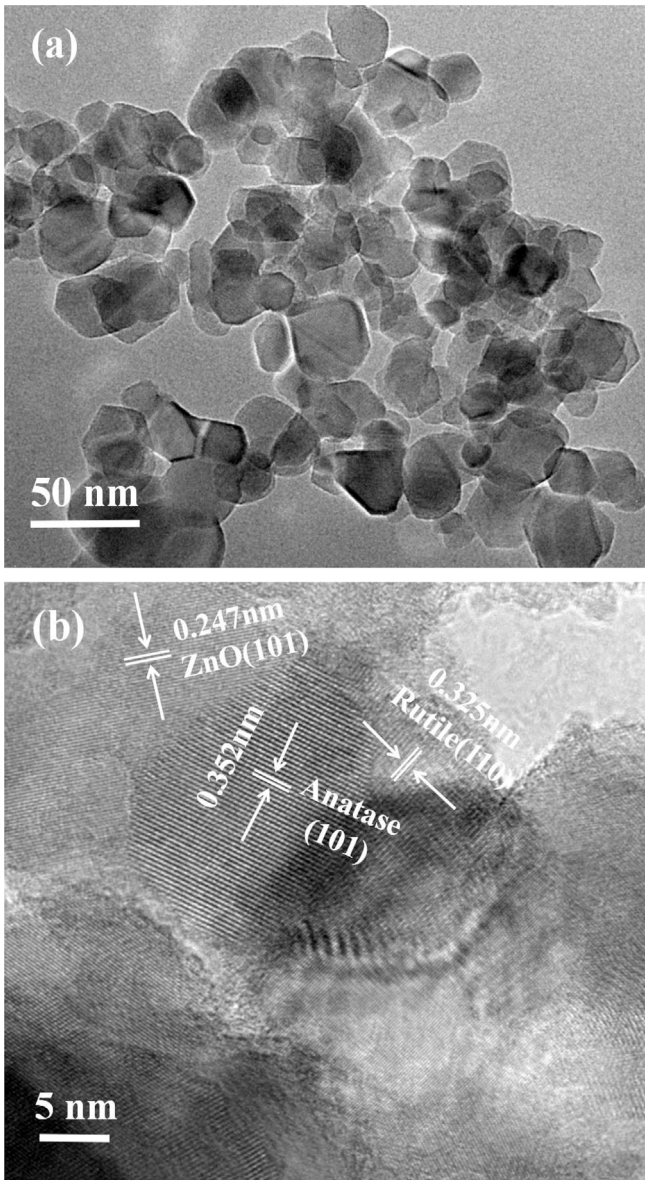

Fig. 3. TEM images of 7at%Zn-TiO_2.

the frequency range of 0.01–10^5 Hz in dark. Typically, the working electrode was prepared as follows: 10 mg of the as-synthesized photocatalysts was mixed with 0.8 mL DMF under sonication for 2 h to form homogeneous emulsion, and then 20 μL of the emulsion was dip-coated onto a 0.5 cm × 0.5 cm FTO glass electrode. After drying at room temperature for 24 h, the uncoated parts of the electrode were covered by epoxy resin.

3. Results and discussion

3.1. Structure and morphology

XRD was employed to investigate the crystal structure and chemical composition of the Zn-TiO_2 samples, and their diffraction patterns were shown in Fig. 1. The peaks centered at 25.3°, 37.8° and 48.0° could be indexed to the (101), (004) and (200) planes of anatase TiO_2 (PDF$^{\#}$21-1272), respectively. The other ones at 27.4° and 36.1° were derived from (110) and (101) facets of rutile TiO_2 (PDF$^{\#}$21-1276). There is no other phase in the diffraction patterns when the molar ratio of Zn/Ti is lower than 7%, which might be due to the low loading content of Zn species on the surface of TiO_2. In the case of 10at%Zn-TiO_2, there are

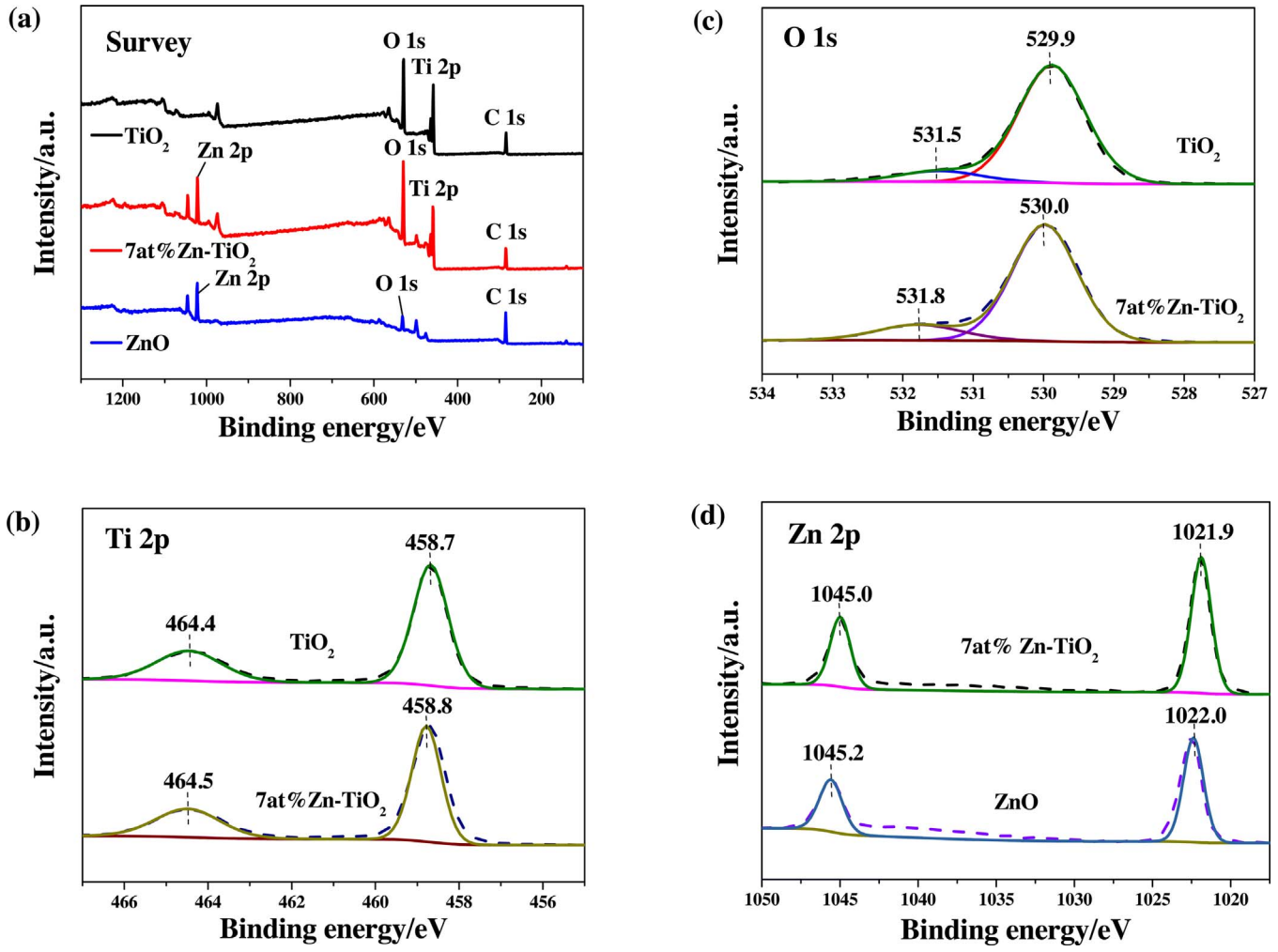

Fig. 4. XPS spectra of TiO_2, 7at%Zn-TiO_2 and ZnO including the survey (a), Ti 2p (b), O 1 s (c) and Zn 2p (d).

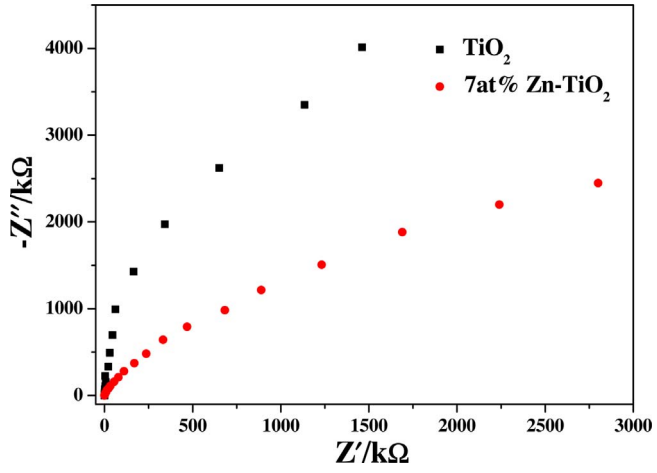

Fig. 5. EIS Nyquist plots of TiO_2 and 7at%Zn-TiO_2 obtained by applying AC amplitude of 10.0 mV over the frequency range of 0.01–10^5 Hz in dark.

three new diffraction peaks (marked with "♣") at 31.8°, 34.4° and 36.3°, corresponding to (100), (002) and (101) lattice planes of ZnO (PDF#36-1451), respectively. This demonstrates that TiO_2 and ZnO are coexisted in the composite.

The morphologies of the synthesized samples were characterized by SEM (Fig. 2a–b). Pure TiO_2 is consisted of nanoparticles with a size distribution ranging from 10 to 40 nm. In the case of 7at%Zn-TiO_2, it is also a particle-like structure, but the nanoparticles tend to aggregate together. The EDS element analysis of 7at%Zn-TiO_2 was also conducted. As shown in Fig. S1 and Fig. S2, Ti, O and Zn elements are clearly detected, and Zn element is well distributed over TiO_2 nanoparticles. The detailed structural information about 7at%Zn-TiO_2 was studied by TEM. Fig. 3a reveals that 7at%Zn-TiO_2 presents a nanoparticle-like appearance with the size of *ca.* 10–40 nm, in accordance with SEM results. As displayed in the typical HRTEM image (Fig. 3b), it is clear to observe the lattice spacing of 0.352 and 0.325 nm, corresponding to the (101) plane of anatase TiO_2 and (110) plane of rutile TiO_2, respectively. Additionally, a lattice fringe with *d*-spacing of 0.247 nm is assigned to the (101) lattice plane of ZnO. These results confirm the existence of ZnO on the surface of TiO_2 and an intimate contact between ZnO and TiO_2 in the composite.

The elemental composition and chemical state of 7at%Zn-TiO_2 were further investigated by X-ray photoelectron spectroscopy (XPS), with pure TiO_2 and ZnO as references. The signals of C, Ti, O and Zn elements are found in the survey spectrum of 7at%Zn-TiO_2 (Fig. 4a). Fig. 4b–d show the comparison data of the XPS Ti 2p, O 1 s and Zn 2p spectra. The Ti 2p spectra of TiO_2 and 7at%Zn-TiO_2 clearly show two peaks at 464.4 and 458.7 eV, associated to the Ti $2p_{1/2}$ and Ti $2p_{3/2}$ characteristic spectrum of Ti^{4+} oxidation state in TiO_2, respectively [31–33]. According to these results, the structure and elemental state of TiO_2 are not changed after modification with ZnO. The O 1 s spectra for TiO_2 and 7at%Zn-TiO_2 can be fitted into two peaks. The peak located at 529.8-530.0 eV is ascribed to the lattice oxygen (O_{lat}) and the other peak at 531.4-531.8 eV is assigned to the surface adsorbed oxygen

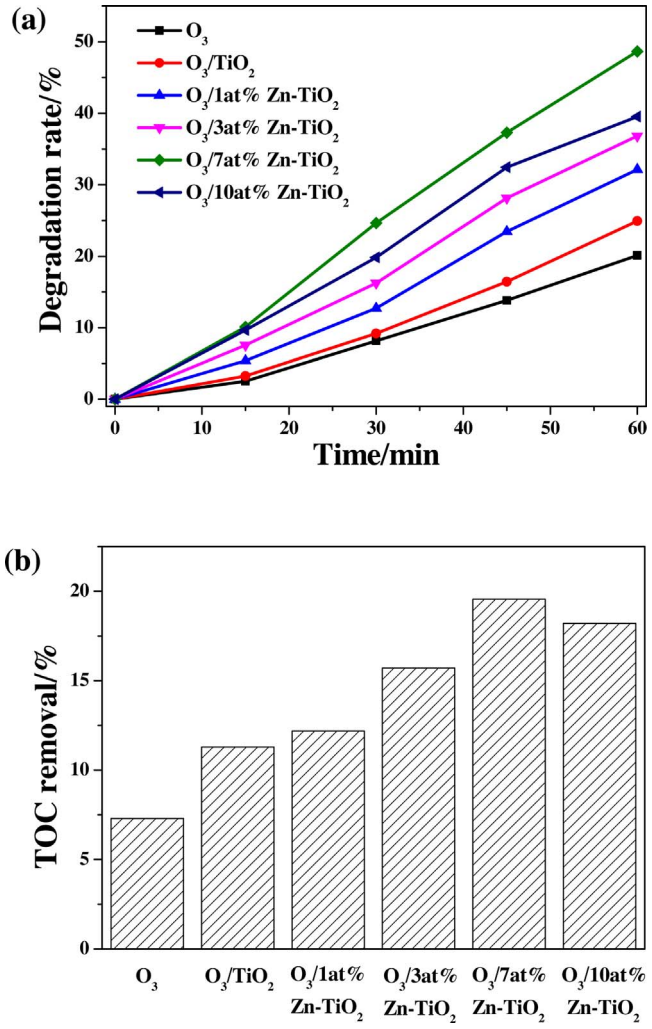

Fig. 6. (a) Degradation rate of SA in ozonation process over Zn-TiO_2 with different Zn/Ti ratio, (b) the corresponding TOC removal of SA. Reaction conditions: $[SA]_0$ = 80 ppm; catalyst loading = 0.5 g/L; ozone flow rate, 30 mL/min; ozone concentration, 5 mg/L; initial solution pH = 3.5.

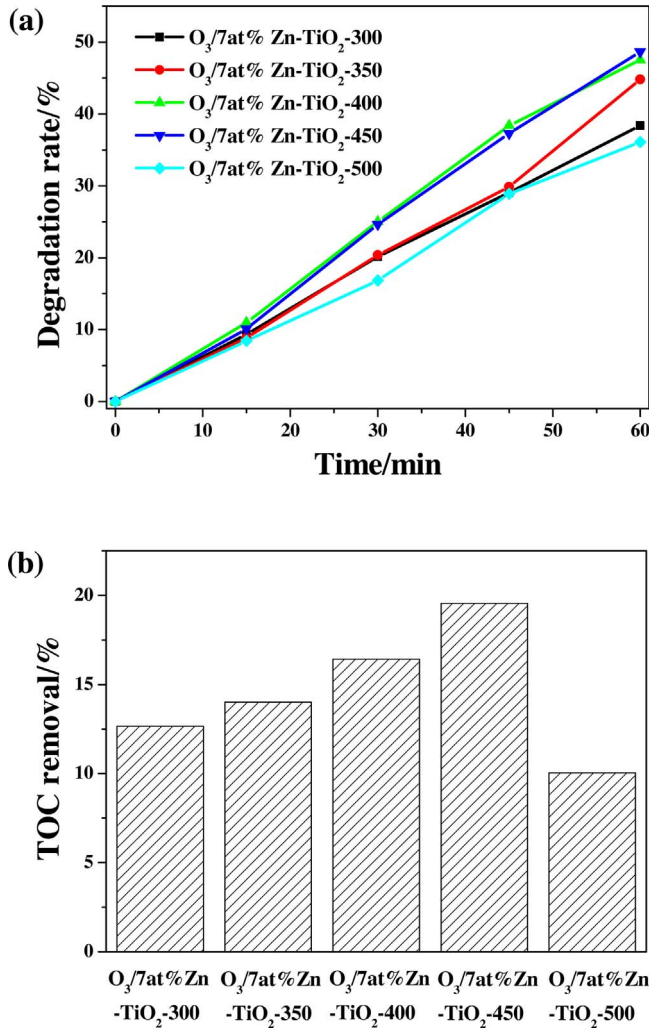

Fig. 7. (a) Degradation rate of SA in ozonation process over Zn-TiO_2 annealed at different temperatures, (b) the corresponding TOC removal of SA. Reaction conditions: $[SA]_0$ = 80 ppm; catalyst loading = 0.5 g/L; ozone flow rate, 30 mL/min; ozone concentration, 5 mg/L; initial solution pH = 3.5.

(O_{ads}) [34–36]. A quantitative analysis on O 1 s XPS spectra could give rise to the molar ratios of O_{ads} and O_{lat}, as summarized in Table S1. It displays that the fraction of O_{ads} (surface hydroxyl group) for 7at%Zn-TiO_2 is higher than that of TiO_2, which is advantageous to the photo-induced charge transfer, resulting in a high catalytic activity [28,36]. Finally, in the case of the Zn 2p spectra, it presents double peaks at 1045.0 and 1021.9 eV, corresponding to Zn $2p_{1/2}$ and Zn $2p_{3/2}$ characteristic spectrum of Zn^{2+} oxidation state, respectively [37]. The XPS results further verify the coexistence of ZnO and TiO_2 in the 7at%Zn-TiO_2 composite.

In order to investigate the effect of ZnO modification on the surface area and pore structure of TiO_2, the N_2 adsorption-desorption isotherms were measured (Fig. S3), and the textural parameters derived from the isotherms data were summarized in Table S2. 1at%Zn-TiO_2 has similar surface area and pore volume compared with pure TiO_2. However, further increasing the ratio of Zn/Ti in the sample can slightly decrease the surface area and pore volume. 7at%Zn-TiO_2 has a surface area of 44.1 m^2/g, lower than that of pure TiO_2 (54.6 m^2/g). This can be ascribed to the aggregation of nanoparticles when ZnO is loaded onto the surface of TiO_2 [36,38].

3.2. Electrochemical properties

The electrochemical impedance spectroscopy (EIS) has been widely utilized to investigate the transfer of interface charge carriers [30,38,39]. As shown in EIS Nyquist plots (Fig. 5), 7at%Zn-TiO_2 has a smaller arc radius than TiO_2. Generally, the smaller arc radius means the faster rate of the interface charge carriers transfer [38,39]. Thus it can be deduced that 7at%Zn-TiO_2 has an improved transfer behavior for the photoexcited carriers.

Transient photocurrent response was also used to evaluate the separation efficiency of photogenerated electron-hole for 7at%Zn-TiO_2 and TiO_2. Fig. S4 displays their photocurrent-time curves during repeated ON/OFF irradiation cycles. 7at%Zn-TiO_2 has a higher photocurrent than TiO_2, implying that 7at%Zn-TiO_2 exhibits a higher efficiency in the photogenerated charges separation than TiO_2. This will be beneficial to enhance the activity of TiO_2 in the photocatalytic ozonation reaction [40]. Furthermore, the transient photocurrent of 7at%Zn-TiO_2 switch reversibly and reproducibly under the successive periodic illumination, this would be closely connected with its photocatalytic stability [40].

3.3. Ozonation activity

3.3.1. Influence of Zn content on catalytic activity

Fig. 6a displays the degradation rate of SA in catalytic ozonation processes with different catalysts. After reaction for 60 min, the SA degradation rate of individual ozonation is 20.1% and the value

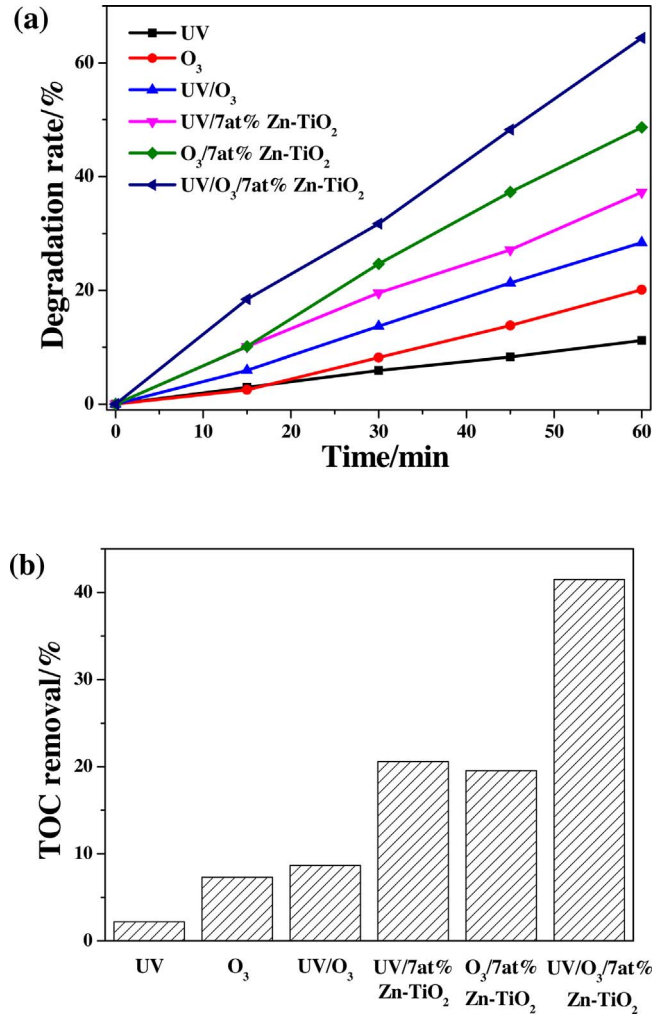

Fig. 8. (a) Degradation rate of SA in different oxidation processes and (b) the corresponding TOC removal of SA. Reaction conditions: $[SA]_0$ = 80 ppm; catalyst loading = 0.5 g/L; ozone flow rate, 30 mL/min; ozone concentration, 5 mg/L; initial solution pH = 3.5.

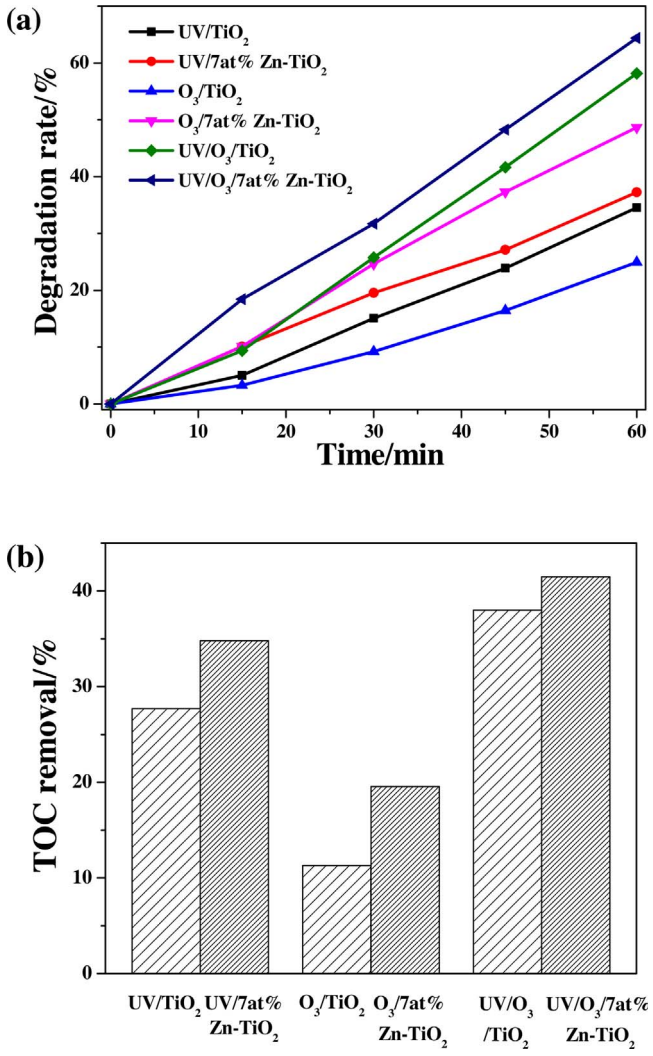

Fig. 9. (a) The comparison of degradation rate of SA over TiO_2 and 7at%Zn-TiO_2 in different oxidation processes and (b) the corresponding TOC removal of SA. Reaction conditions: $[SA]_0$ = 80 ppm; catalyst loading = 0.5 g/L; ozone flow rate, 30 mL/min; ozone concentration, 5 mg/L; initial solution pH = 3.5.

increases to 24.9% in the presence of TiO_2. The catalytic activity for SA degradation over Zn-TiO_2 is found to be strongly dependent on the ratio of Zn/Ti. The degradation rate of SA increases initially and then reaches an optimum when the ratio is about 7.0 at%. Further increasing the ratio of Zn/Ti leads to a decrease in the catalytic activity for SA degradation. Meanwhile, the TOC removal in the catalytic process was also measured. As shown in Fig. 6b, 7at%Zn-TiO_2 exhibits the best catalytic performance for SA mineralization. Combining with the characterization results of the Zn-TiO_2, it can be concluded that catalytic activities of the samples might be closely related to the amounts of surface hydroxyl groups rather than their surface specific areas [36].

3.3.2. *Effect of calcination temperature on catalytic activity*

The influence of the calcination temperature of 7at%Zn-TiO_2 on the catalytic performance was also studied and the result was shown in Fig. 7. When the calcination temperature of 7at%Zn-TiO_2 precursor increases from 300 to 450 °C, the degradation rate of SA increases from 38.4% to 48.6%, accordingly (Fig. 7a). Notably, when the calcination temperature further increases to 500 °C, the degradation rate decreases to 36.1%, suggesting that 7at%Zn-TiO_2-450 exhibits the highest catalytic performance among these samples obtained at different temperatures. This is well consistent with the results of TOC removal as shown in Fig. 7b. Therefore, 7at%Zn-TiO_2 nanocomposite annealed at 450 °C is adopted for subsequent studies.

3.4. *Comparison of different oxidation processes in the degradation of SA*

The catalytic activity of 7at%Zn-TiO_2 was ascertained by monitoring the degradation and mineralization of SA in different oxidation processes. As shown in Fig. 8a, the degradation rate of SA is 11.2% for direct photolysis under UV light irradiation and 20.1% for ozonation alone. The presence of UV light or 7at%Zn-TiO_2 in ozonation process increases SA degradation efficiency, and 28.4% and 48.6% of SA are removed using UV/O_3 and O_3/7at%Zn-TiO_2, respectively. For comparison, the SA degradation over 7at%Zn-TiO_2 under UV light irradiation is also evaluated, and 37.2% of SA is decomposed after reacting for 60 min. When photocatalysis and ozonation are performed simultaneously, 64.4% of SA is removed by using 7at%Zn-TiO_2 as the catalyst, which is higher than the sum of those in UV/7at%Zn-TiO_2 and O_3. This enhancement is attributed to a synergistic effect between photocatalysis and ozonation. The results of TOC removal (Fig. 8b) also confirm the synergy between photocatalysis and ozonation. Among the above six processes, UV/O_3/7at%Zn-TiO_2 achieves the highest efficiency of SA degradation and mineralization.

The catalytic efficiency of 7at%Zn-TiO_2 and pure TiO_2 were compared through the degradation and mineralization of SA, and the results were presented in Fig. 9. It can be seen that 7at%Zn-TiO_2 exhibits a higher photocatalytic activity than TiO_2 under UV light illumination.

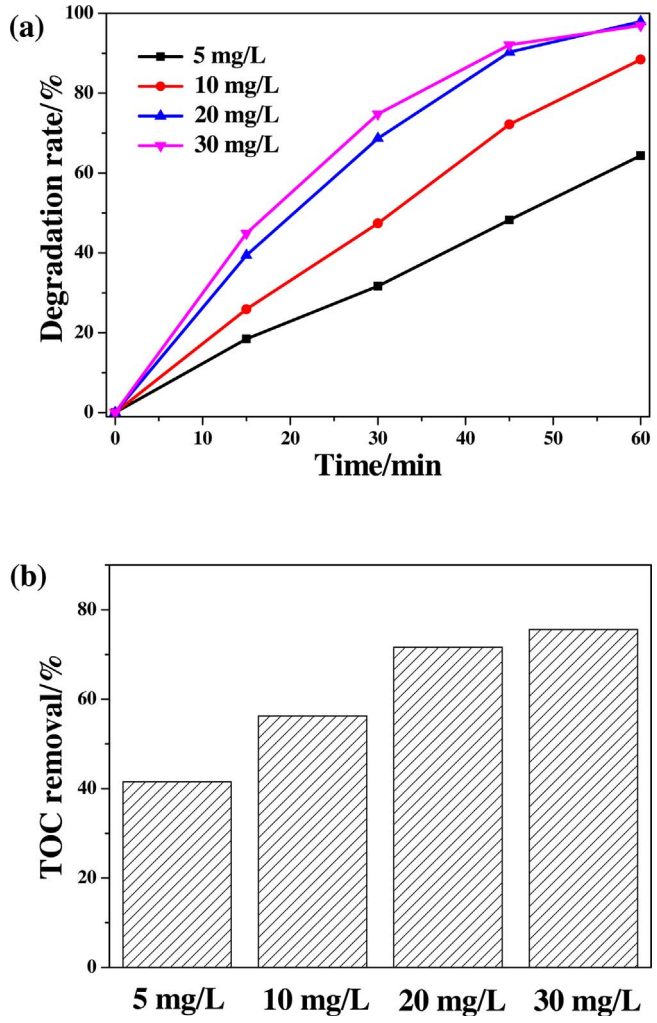

Fig. 10. (a) Effect of ozone concentration on the degradation rate of SA by 7at%Zn-TiO_2 in photocatalytic ozonation process and (b) the corresponding TOC removal of SA. Reaction conditions: $[SA]_0$ = 80 ppm; catalyst loading = 0.5 g/L; ozone flow rate, 30 mL/min; initial solution pH = 3.5.

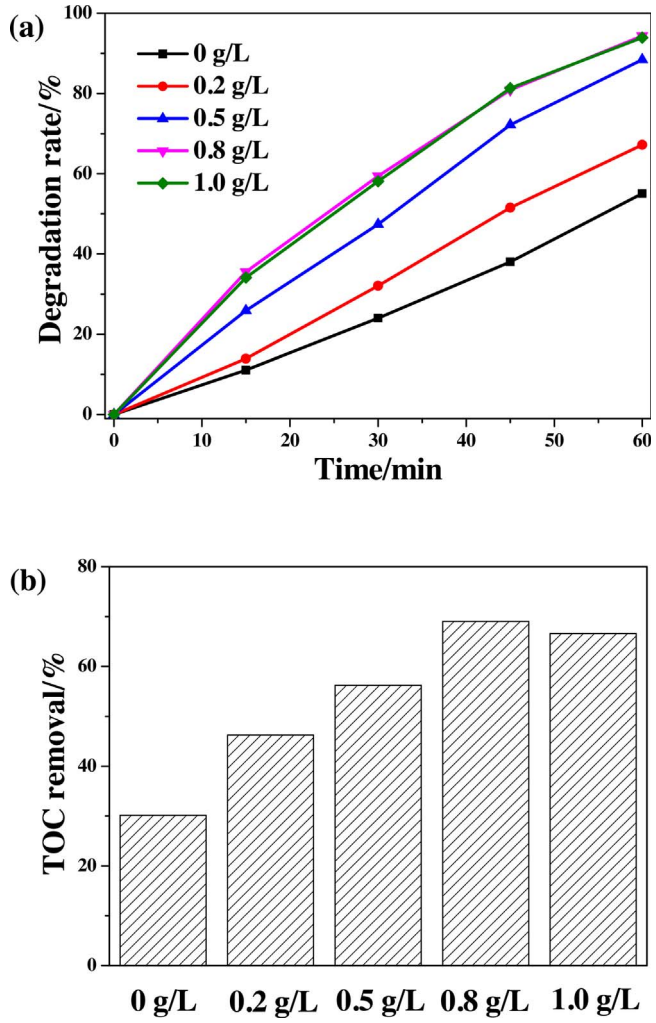

Fig. 11. (a) Effect of catalyst dosage on the degradation rate of SA in photocatalytic ozonation process and (b) the corresponding TOC removal of SA. Reaction conditions: $[SA]_0$ = 80 ppm; ozone flow rate, 30 mL/min; ozone concentration, 10 mg/L; initial solution pH = 3.5.

The degradation rate in ozonation by 7at%Zn-TiO_2 is 48.6%, which is about two times as high as that by TiO_2. UV/O_3/7at%Zn-TiO_2 also shows a higher efficiency in TOC removal than UV/O_3/TiO_2 for SA mineralization.

3.5. Influence of parameters on photocatalytic ozonation

3.5.1. Effect of ozone concentration

The photocatalytic ozonation degradation of SA with varied ozone concentration was measured to disclose the role of ozone in the combined process. As seen in Fig. 10, both degradation rate and TOC removal are greatly improved when ozone concentration increases from 5 to 20 mg/L. Nevertheless, further increase of ozone concentration does not significantly enhance the removal efficiency. In generally, ozone is considered as an efficient scavenger for the photogenerated electrons, which can remarkably accelerate charge separation in photocatalysis reactions [10–12]. The ozone is insufficient to capture photogenerated electrons when the ozone concentration is below 20 mg/L, while the ozone concentration of 30 mg/L could well match the generation rate of electrons over 7at%Zn-TiO_2. The procedure of trapping photoinduced electrons by ozone is vital because it facilitates charge-carrier transfer and ozone decomposition, which synergistically accelerates the formation of more active species in the reaction [10–12].

3.5.2. Effect of catalyst dosage

The appropriate catalyst concentration is of great importance for the practical applications, thus the influence of catalyst dosage on catalytic activity was investigated. As illustrated in Fig. 11, when the amount of 7at%Zn-TiO_2 used in the photocatalytic ozonation system increases from 0 to 0.8 g/L, the degradation rate of SA promotes from 55.0% to 94.4% and the TOC removal enhances from 30.2% to 69.0% during the reaction time of 60 min, owing to higher exposed areas and more active sites of 7at%Zn-TiO_2 that are available for SA adsorption and mineralization. However, there has negligible change in degradation rate and TOC removal when the catalyst dosage further increases to 1.0 g/L, meaning that the overdose of catalyst cannot further significantly improve the degradation rate and TOC removal of SA.

3.5.3. Effect of initial SA concentration

The initial pollutant concentration plays an important role on the catalytic activity of catalyst. The influence of initial SA concentration was explored ranging from 40 to 120 ppm and the results were shown in Fig. 12. The degradation rate and TOC removal drastically decrease when the initial SA concentration increases from 40 to 120 ppm. Two factors may be responsible for this phenomenon: On one hand, most of the photocatalytic ozonation reactions follow the LH equation [41], thus the catalytic active sites will be occupied by pollutant at a high initial concentration. On the other hand, a higher initial concentration

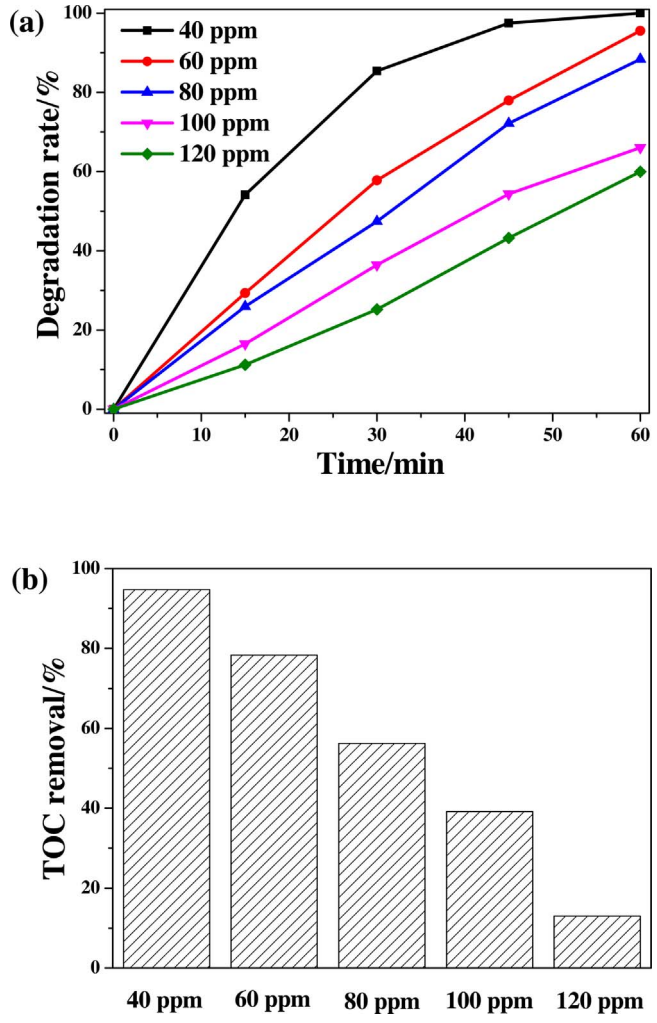

Fig. 12. (a) Effect of initial concentration of SA solution on the degradation rate of SA by 7at%Zn-TiO_2 in photocatalytic ozonation process and (b) the corresponding TOC removal of SA. Reaction conditions: catalyst loading = 0.5 g/L; ozone flow rate, 30 mL/min; ozone concentration, 10 mg/L.

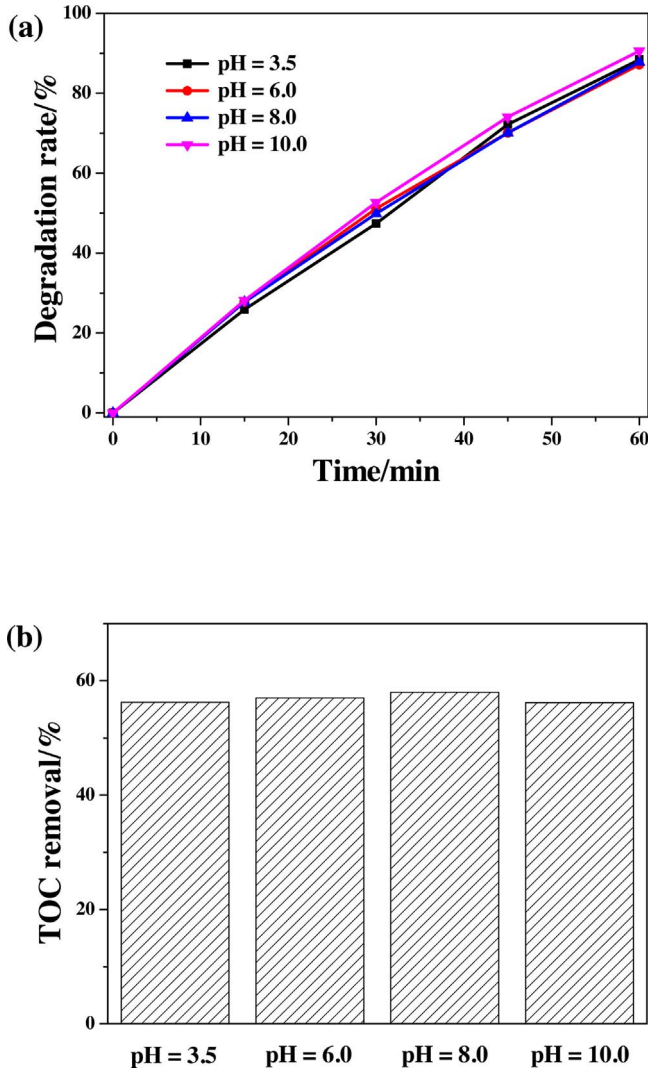

Fig. 13. (a) Effect of solution pH on the degradation rate of SA in photocatalytic ozonation process by 7at%Zn-TiO_2 and (b) the corresponding TOC removal of SA. Reaction conditions: $[SA]_0$ = 80 ppm; catalyst loading = 0.5 g/L; ozone flow rate, 30 mL/min; ozone concentration, 10 mg/L.

will yield a higher concentration of intermediates adsorbed on the catalyst, which can influence the overall decomposition and mineralization rates [41].

3.5.4. Effect of initial solution pH

pH value of aqueous solution is a crucial factor which affects the evolution of hydroxyl radicals and the utilization efficiency of ozone [42,43]. Fig. 13 displays the influence of initial pH (3.5, 6.0, 8.0, 10.0) of aqueous solution on SA decomposition and mineralization in UV/O_3/7at%Zn-TiO_2 process. No obvious difference in the degradation rate and mineralization is observed when the solution pH is adjusted to the considered pH values. It suggests that 7at%Zn-TiO_2 nanocomposite exhibits good catalytic performance in both acidic and alkaline conditions [28], demonstrating its great potential in practical wastewater treatment.

3.5.5. Effect of inorganic ion

Inorganic ions such as Na^+, Ca^{2+}, K^+, Cl^-, NO_3^- and CO_3^{2-} commonly exist in the wastewater. The effects of these ions on photocatalytic ozonation of SA were investigated. The SA removal efficiencies at different ions are given in Fig. 14. It is found that the degradation rate of SA at 60 min reaches almost 88.4% in the absence of any ion in UV/O_3/7at%Zn-TiO_2 process. The addition of Na^+ and Cl^- appears to have a negligible effect on SA removal. Nevertheless, the catalytic activity of 7at%Zn-TiO_2 is slightly inhibited in the presence of Ca^{2+}, K^+ or NO_3^-. Moreover, the catalytic activity is remarkably reduced in the presence of CO_3^{2-}, and the degradation rate decreases to 65.8%. It is assumed that Ca^{2+}, K^+, NO_3^- and CO_3^{2-} are the scavengers of the active species [44,45], which can account for the decrease of SA removal in the photocatalytic ozonation process when the system is added with Ca^{2+}, K^+, NO_3^- or CO_3^{2-}.

3.6. Mechanism discussion of photocatalytic ozonation process

Electron paramagnetic resonance (EPR) experiments were performed by using 7at%Zn-TiO_2 as the catalyst to identify the possible active species generated for SA degradation and mineralization to elucidate the photocatalytic ozonation mechanism. In order to detect ·OH and $\cdot O_2^-$, 5, 5-dimethyl-1-pyrroline (DMPO) was served as the radical scavenger in EPR experiments by measuring the signals of DMPO/·OH and DMPO/$\cdot O_2^-$ species [46–51]. In addition, 2, 2, 6, 6-tetramethyl-4-piperidinol (TEMP) was adopted as the spin-trapping agent to detect $^1O_2$ [46]. EPR experiments were performed in ultrapure water for ·OH detection. Four-line spectra with the relative intensity of 1:2:2:1 are obviously observed in the UV/O_3 and UV/O_3/7at%Zn-TiO_2 processes (Fig. 15a), which are deemed to be the characteristic spectra

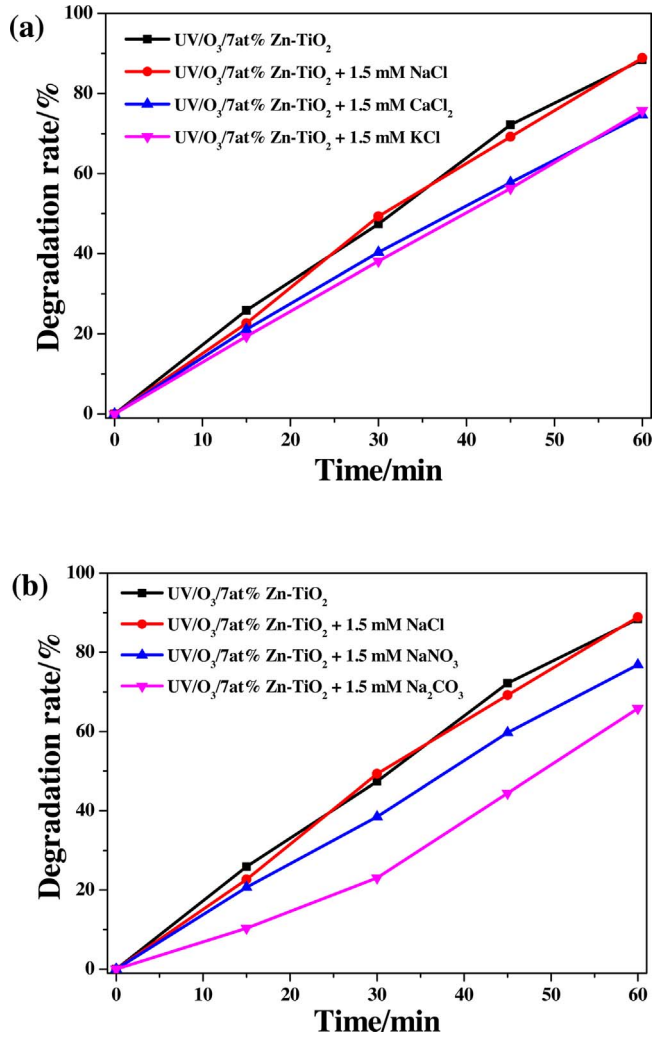

Fig. 14. Effect of different ions in SA solution on the degradation rate of SA by 7at%Zn-TiO_2 in photocatalytic ozonation process: (a) cations and (b) anions. Reaction conditions: $[SA]_0$ = 80 ppm; catalyst loading = 0.5 g/L; ozone flow rate, 30 mL/min; ozone concentration, 10 mg/L.

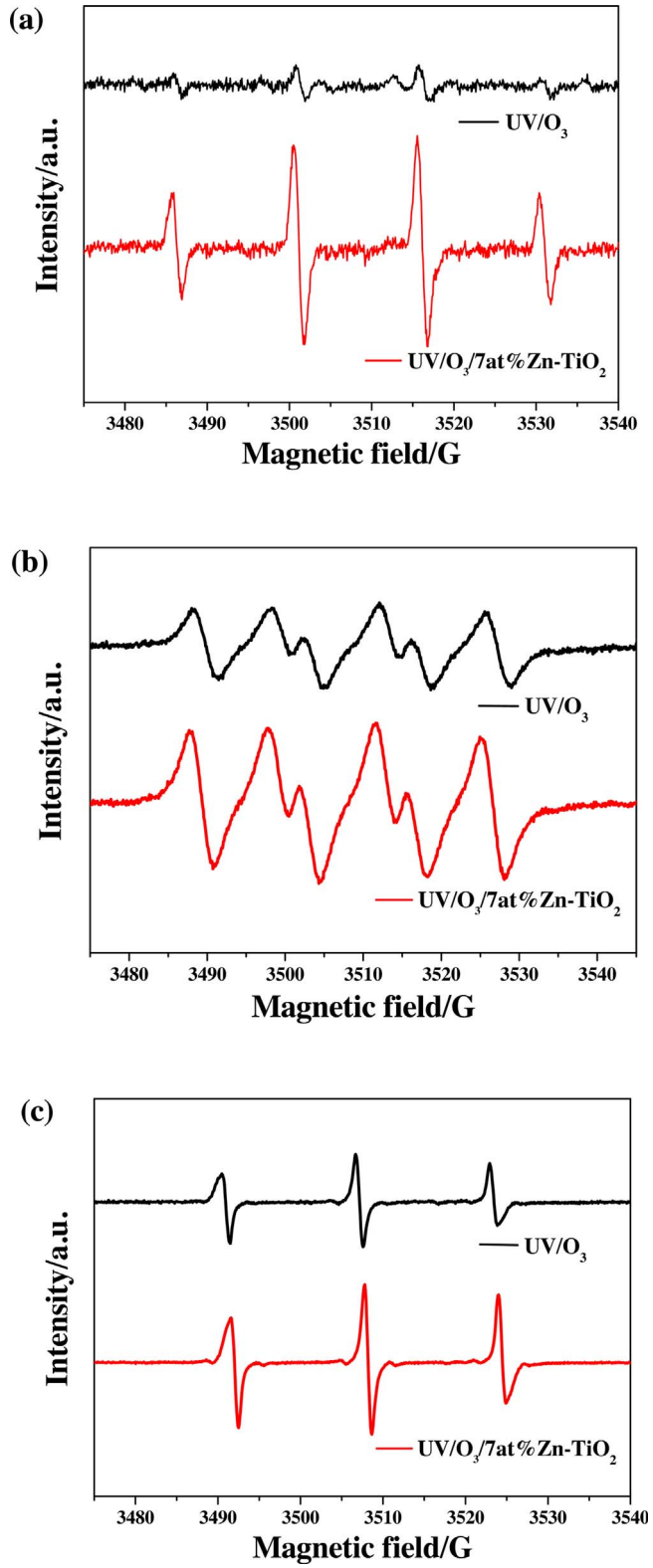

Fig. 15. EPR spectra of DMPO/·OH (a), DMPO/$\cdot O_2^-$ (b) and TEMP/$^1O_2$ adducts (c) over the systems of UV/O_3 and UV/O_3/7at%Zn-TiO_2. Reaction conditions: ozone flow rate, 30 mL/min; ozone concentration, 10 mg/L; catalyst loading = 2 g/L; liquid volume: 10 mL; reaction time, 10 min.

of DMPO/·OH [47–49]. When compared to counterpart in the UV/O_3 process, the intensity of DMPO/·OH signal is conspicuously enhanced in UV/O_3/7at%Zn-TiO_2 process. For the detection of $\cdot O_2^-$, absolute methanol was used as the reaction medium instead of ultrapure water. The EPR signals of four-line spectra with the relative intensity of 1:1:1:1 assigning to DMPO/$\cdot O_2^-$ adducts are observed in both processes (Fig. 15b) [50,51], and the intensity of DMPO/$\cdot O_2^-$ signal is remarkably boosted when the UV/O_3 system introduces 7at%Zn-TiO_2 as a catalyst. Moreover, the radical of singlet oxygen $^1O_2$ was tested by EPR with the sensitive probe of TEMP. The observed three-line spectrum with equal intensities is a characteristic of the formed TEMP/$^1O_2$ adduct (TEMPO) [46]. Similar EPR spectra are observed in the UV/O_3 and UV/O_3/7at%Zn-TiO_2 system (Fig. 15c), and stronger characteristic signal is viewed in the photocatalytic ozonation process with the addition of 7at%Zn-TiO_2. All these results reveal that ·OH, $\cdot O_2^-$ and $^1O_2$ are the active species during the UV/O_3 and UV/O_3/7at%Zn-TiO_2 processes. The amount of the active species is enhanced during the combined system with 7at%Zn-TiO_2, which could facilitate the decomposition and mineralization of SA.

To further confirm the contribution of the active species to the SA degradation, the radical trapping experiments using 7at%Zn-TiO_2 composite as the catalyst were carried out. *tert*-butanol (TBA) and ammonium oxalate (AO) is believed to be the effective scavengers for · OH [52,53] and h^+ [47,54], separately. As depicted in Fig. S5, the degradation rate of SA at 60 min reaches almost 88.4% in the absence of AO and TBA in UV/O_3/7at%Zn-TiO_2 process. However, the removal rate of SA within 60 min dramatically decreases to 56.3% and 71.7% in

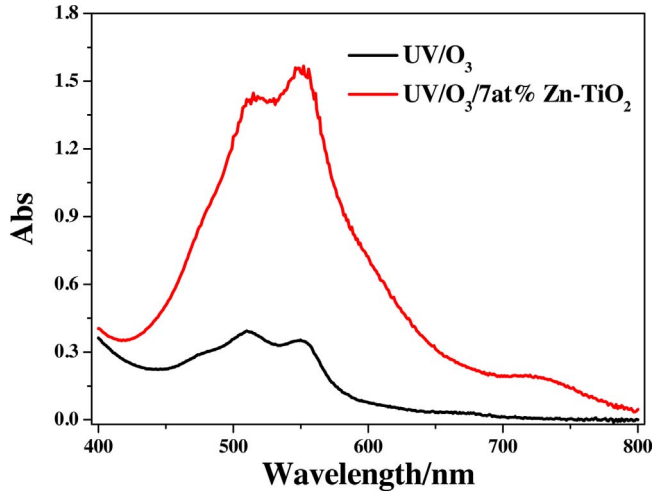

Fig. 16. UV–vis spectra of H_2O_2 generated in UV/O_3 and UV/O_3/7at%Zn-TiO_2 process. Reaction conditions: $[SA]_0$ = 80 ppm; catalyst loading = 0.5 g/L; ozone flow rate, 30 mL/min; ozone concentration, 10 mg/L; initial solution pH = 3.5.

the presence of 1 mM AO and 1 mM TBA, respectively. This denotes that both h^+ and ·OH contribute to the decomposition of SA, which is in good agreement with the EPR results. In addition, H_2O_2 is identified as another kind of active species in the chain reaction in the photocatalytic ozonation process. N, N-diethyl-*p*-phenylendiamine (DPD) method was adopted to detect H_2O_2 [51,55–57] and the results were shown in Fig. 16. The characteristic absorption intensity of H_2O_2 generated in the photocatalytic ozonation system with 7at%Zn-TiO_2 in 60 min is notably higher than that in UV/O_3 process, suggesting that 7at%Zn-TiO_2 composite accelerates the evolution of H_2O_2 [51,57].

3.7. Investigation of SA mineralization pathway

The intermediates of SA in UV/O_3/7at%Zn-TiO_2 process were further detected by HPLC–MS to reveal the mineralization process. Fig. S6 shows the ESI–MS spectra of initial SA, intermediates in UV/O_3/7at% Zn-TiO_2 at 15, 30, 45 and 60 min. On the basis of these results, the main by-products generated during the reaction process were identified. Fig. 17 delineates the intermediate products and the proposed SA mineralization pathway during the photocatalytic ozonation process. The aromatic ring of SA is firstly electrophilically attacked by the radicals to produce 2, 5-dihydroxybenzoic acid as well as 2, 3-dihydroxybenzoic acid (m/z = 153.0), which further transforms into muconic acid (m/z = 141.0) with ring opening. Subsequently, the non-selective radicals contribute to further mineralization of muconic acid (m/z = 141.0) and maleic/fumaric acid (m/z = 115.0), which converts into CO_2 and H_2O, and the mineralization of SA is fully completed. The intermediate formation process is also verified by the change in the peak intensity of the corresponding compounds (shown in Fig. S6).

3.8. Stability of 7at%Zn-TiO_2 and extensive use for other organics removal

In order to investigate the stability of 7at%Zn-TiO_2 in the photocatalytic ozonation system, 7at%Zn-TiO_2 was recycled for SA degradation. As presented in Fig. 18, the catalytic activity of 7at%Zn-TiO_2 does not decrease obviously after recycling for four times, which is in good agreement with the result of TOC removal, indicative of the good stability of 7at%Zn-TiO_2 for SA removal.

The catalytic performance of 7at%Zn-TiO_2 for phenol and MO mineralization was also evaluated. In the case of phenol degradation (Fig. S7), UV/O_3/7at%Zn-TiO_2 exhibits a TOC removal of 52.5% during 90 min, higher than UV (4.0%), O_3 (3.5%), UV/7at%Zn-TiO_2 (34.4%), UV/O_3 (10.4%) and O_3/7at%Zn-TiO_2 (12.6%). Phenol mineralization efficiency in the photocatalytic ozonation with 7at%Zn-TiO_2 is much higher than the sum of those in UV/7at%Zn-TiO_2 and O_3. This also embodies that the 7at%Zn-TiO_2 triggers a positive synergy between photocatalysis and ozonation. In regard to methyl orange (MO) removal, similar results are also obtained (Fig. S8). About 25.9% of TOC is removed by photocatalytic ozonation with 7at%Zn-TiO_2 in 60 min, which is also much higher than the sum of those in single photocatalysis and ozonation. This result further affirms the presence of synergistic performance between photocatalysis and ozonation to improve the catalytic activity. The above results demonstrate that 7at%Zn-TiO_2 possesses good catalytic activity and stability for organic contaminants removal.

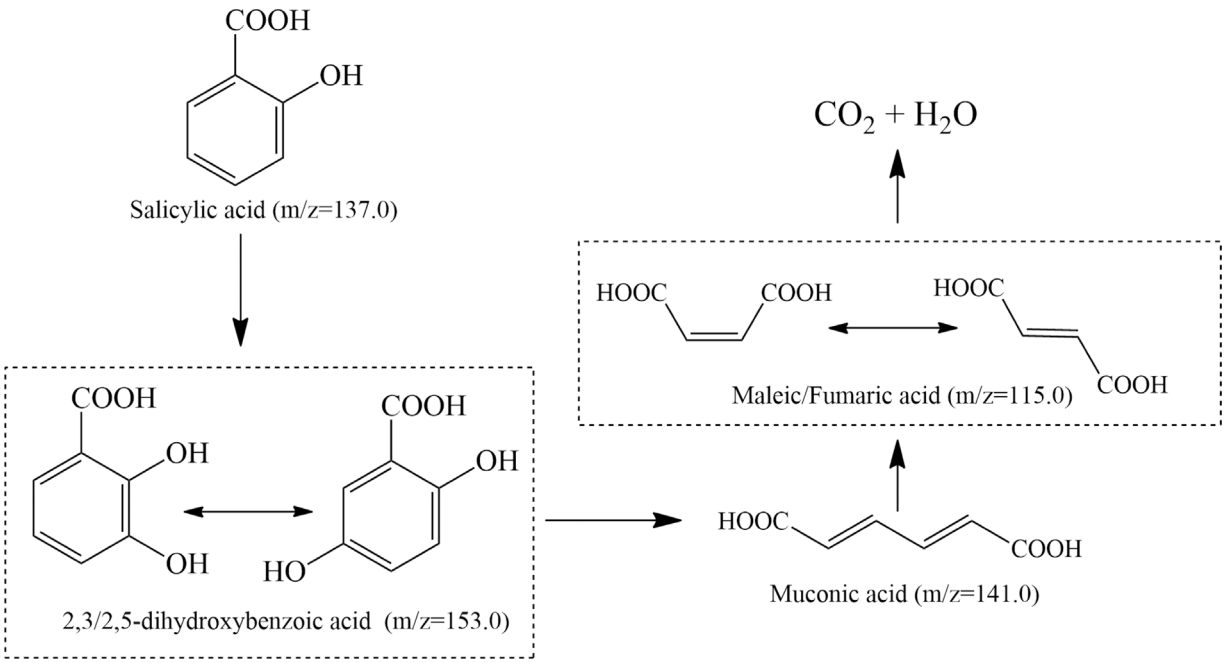

Fig. 17. A possible pathway for SA mineralization in UV/O_3/7at%Zn-TiO_2 process.

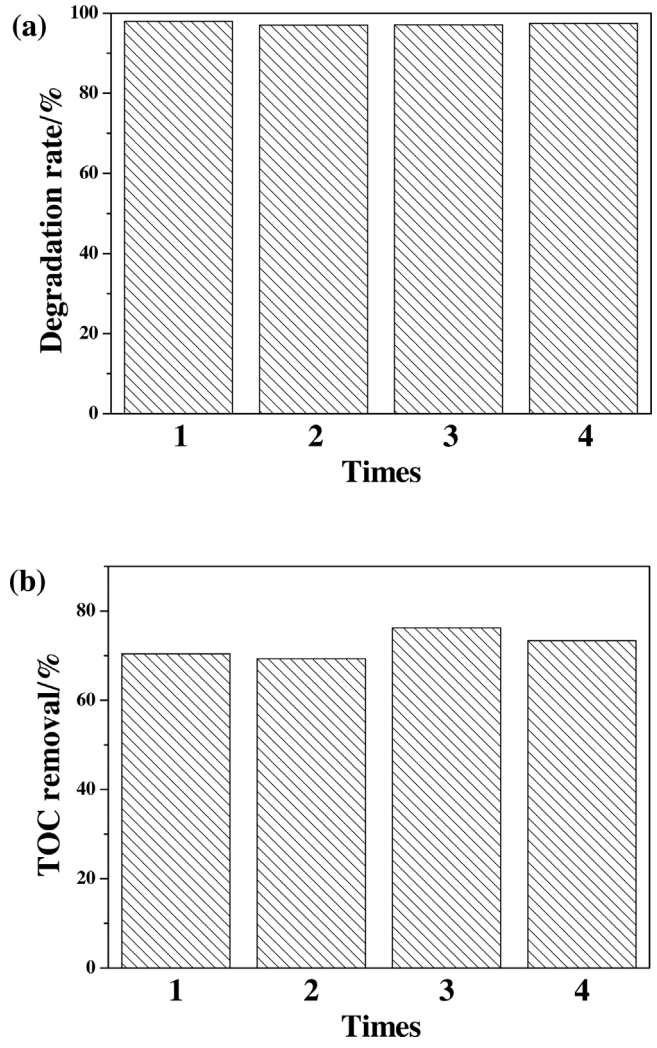

Fig. 18. (a) The degradation rate of SA and (b) the corresponding TOC removal in 90 min by 7at%Zn-TiO_2 photocatalytic ozonation reaction for four cycles. Reaction conditions: $[SA]_0$ = 80 ppm; catalyst loading = 0.5 g/L; ozone flow rate, 30 mL/min; ozone concentration, 10 mg/L; initial solution pH = 3.5.

4. Conclusion

In summary, ZnO-TiO_2 nanocomposites were successfully synthesized via a simple impregnation-calcination method and employed to the photocatalytic ozonation decomposition of organic contaminants. The 7at%Zn-TiO_2 exhibited enhanced catalytic performance in both SA degradation and mineralization, which was attributed to the richer surface hydroxyl groups and higher separation efficiency of photogenerated electron-holes. The 7at%Zn-TiO_2 also triggered a synergy between photocatalysis and ozonation for pollutants (SA, phenol and MO) mineralization. Mechanism studies revealed that H_2O_2, h^+, ·OH, $\cdot O_2^-$ and $^1O_2$ were the main active species to drive the reaction for pollutants removal. Moreover, the 7at%Zn-TiO_2 displayed good stability in the combined process and could be applied in a wide pH range of aqueous solution. This investigation might provide some guidance in developing more efficient catalyst and supply a feasible approach for water decontamination.

Acknowledgement

The authors greatly appreciate the financial support from National Key Technologies R & D Program of China (2014BAC13B03), the major science and technology project of Fujian Province (2015YZ0001-1), and the Award Program for Outstanding Young Innovative Talent of Fujian province (00332111)

Appendix A. Supplementary data

Supplementary data associated with this article can be found, in the online version, at http://dx.doi.org/10.1016/j.apcatb.2017.09.025.

References

[1] X. Duan, H. Sun, Y. Wang, J. Kang, S. Wang, ACS Catal. 5 (2015) 553–559.
[2] V. Maroga Mboula, V. Héqueta, Y. Andrès, Y. Gru, R. Colin, Appl. Catal. B: Environ. 162 (2015) 437–444.
[3] N.G. Moustakas, F.K. Katsaros, A.G. Kontos, G. Em Romanos, D.D. Dionysiou, P. Falaras, Catal. Today 224 (2014) 56–69.
[4] T.E. Agustina, H.M. Ang, V.K. Vareek, J. Photochem. Photobiol. C: Photochem. Rev. 6 (2005) 264–273.
[5] U. Černigoj, U.L. Štangar, P. Trebše, Appl. Catal. B: Environ. 75 (2007) 229–238.
[6] M. Mehrjouei, S. Müller, D. Möller, Chem. Eng. J. 263 (2015) 209–219.
[7] L.S. Li, W.P. Zhu, P.Y. Zhang, Z.Y. Chen, W.Y. Han, Water Res. 37 (2003) 3646–3651.
[8] R.R. Giri, H. Ozaki, T. Ishida, Chemosphere 66 (2007) 1610–1617.
[9] M. Mehrjouei, S. Müller, D. Möller, J. Photochem. Photobiol. A: Chem. 217 (2011) 417–424.
[10] G.Z. Liao, D.Y. Zhu, L.S. Li, B.Y. Lan, J. Hazard. Mater. 280 (2014) 531–535.
[11] J.D. Xiao, Y.B. Xie, F. Nawaz, Y.X. Wang, P.H. Du, H.B. Cao, Appl. Catal. B: Environ. 183 (2016) 417–425.
[12] Y. Ling, G.Z. Liao, Y.H. Xie, J. Yin, J.Y. Huang, W.H. Feng, L.S. Li, J. Photochem. Photobiol. A: Chem. 329 (2016) 280–286.
[13] M.M. Ye, Z.L. Chen, X.W. Liu, Y. Ben, J.M. Shen, J. Hazard. Mater. 167 (2009) 1021–1027.
[14] Y. Jing, L.S. Li, Q.Y. Zhang, P. Lu, P.H. Liu, X.H. Lü, J. Hazard. Mater. 189 (2011) 40–47.
[15] H. Ghouas, B. Haddou, M. Kameche, Z. Derriche, C. Gourdon, J. Hazard. Mater. 205-206 (2012) 171–178.
[16] L.B. Reutergådh, M. Iangphasuk, Chemosphere 35 (1997) 585–596.
[17] H. Hao, J. Zhang, Microporous Mesoporous Mater. 121 (2009) 52–57.
[18] Y. Xu, Y.P. Mo, J. Tian, P. Wang, H.G. Yu, J.G. Yu, Appl. Catal. B: Environ. 181 (2016) 810–817.
[19] P. Wang, J. Wang, X.F. Wang, H.G. Yu, J.G. Yu, M. Lei, Y.G. Wang, Appl. Catal. B: Environ. 132–133 (2013) 452–459.
[20] Y.N. Huo, X.F. Chen, J. Zhang, G.F. Pan, J.P. Jia, H.X. Li, Appl. Catal. B: Environ. 148–149 (2014) 550–556.
[21] G. Marci, V. Augugliaro, M.J. López-Munoz, C. Martin, L. Palmisano, V. Rives, M. Schiavello, R.J.D. Tilley, A.M. Venezia, J. Phys. Chem. B 105 (2001) 1033–1040.
[22] J.L. Li, L. Liu, Y. Yu, Y.W. Tang, H.L. Li, F.P. Du, Electrochem. Commun. 6 (2004) 940–943.
[23] X.Z. Li, F.B. Li, C.L. Yang, W.K. Ge, J. Photochem. Photobiol. A: Chem. 141 (2001) 209–217.
[24] Y.R. Do, W. Lee, K. Dwight, A. Wold, J. Solid State Chem. 108 (1994) 198–201.
[25] X.Z. Fu, L.A. Clark, Q. Yang, M.A. Anderson, Environ. Sci. Technol. 30 (1996) 647–653.
[26] Y.K. Takahashi, P. Ngaotrakanwiwat, T. Tatsuma, Electrochim. Acta 49 (2004) 2025–2029.
[27] J. Papp, S. Soled, K. Dwight, A. Wold, Chem. Mater. 6 (1994) 496–500.
[28] H. Zhao, Y.M. Dong, P.P. Jiang, G.L. Wang, J.J. Zhang, C. Zhang, Chem. Eng. J. 260 (2015) 623–630.
[29] T. Ozge, I. Hatice, D. Anatoli, Sep. Sci. Technol. 52 (2017) 778–786.
[30] H. Bashiri, M. Rafiee, Ultrason. Sonochem. 36 (2017) 517–526.
[31] X.Z. Zheng, D.Z. Li, X.F. Li, J. Chen, C.S. Cao, J.L. Fang, J.B. Wang, Y.H. He, Y. Zheng, Appl. Catal. B: Environ. 168–169 (2015) 408–415.
[32] Y. Zhang, P. Zhang, Y.N. Huo, D.Q. Zhang, G.S. Li, H.X. Li, Appl. Catal. B: Environ. 115–116 (2012) 236–244.
[33] H.G. Yu, W.Y. Chen, X.F. Wang, Y. Xu, J.G. Yu, Appl. Catal. B: Environ. 187 (2016) 163–170.
[34] Y. Yang, S.Z. Zhang, S.W. Wang, K.L. Zhang, H.Z. Wang, J. Huang, S.B. Deng, B. Wang, Y.J. Wang, G. Yu, Environ. Sci. Technol. 49 (2015) 4473–4480.
[35] F. Wang, H. Dai, J. Deng, G. Bai, K. Ji, Y. Liu, Environ. Sci. Technol. 46 (2012) 4034–4041.
[36] J.G. Yu, H.G. Yu, B. Cheng, M.H. Zhou, X.J. Zhao, J. Mol. Catal. A-Chem. 253 (2006) 112–118.
[37] P.Y. Kuang, Y.Z. Su, G.F. Chen, Z. Luo, S.Y. Xing, N. Li, Z.Q. Liu, Appl. Surf. Sci. 358 (2015) 296–303.
[38] J.D. Xiao, Y.B. Xie, F. Nawaz, S. Jin, F. Duan, M.J. Li, H.B. Cao, Appl. Catal. B: Environ. 181 (2016) 420–428.
[39] M. Zhang, X.J. Bai, D. Liu, J. Wang, Y.F. Zhu, Appl. Catal. B: Environ. 164 (2015) 77–81.
[40] Q. Liu, Y.R. Guo, Z.H. Chen, Z.G. Zhang, X.M. Fang, Appl. Catal. B: Environ. 183 (2016) 231–241.
[41] O. Carp, C.L. Huisman, A. Reller, Prog. Solid State Chem. 32 (2004) 33–177.
[42] B. Kasprzyk-Hordern, M. Ziólek, J. Nawrocki, Appl. Catal. B: Environ. 46 (2003) 639–669.
[43] L. Zhao, J. Ma, Z. Sun, X. Zhai, Environ. Sci. Technol. 42 (2008) 4002–4007.

[44] J.H. Bing, L.S. Li, B.Y. Lan, G.Z. Liao, J.Y. Zeng, Q.Y. Zhang, X.K. Li, Appl. Catal. B: Environ. 115–116 (2012) 16–24.
[45] C.D. Qi, X.T. Liu, J. Ma, C.Y. Lin, X.W. Li, H.J. Zhang, Chemosphere 151 (2016) 280–288.
[46] Y.X. Wang, Y.B. Xie, H.Q. Sun, J.D. Xiao, H.B. Cao, S.B. Wang, ACS Appl. Mater. Inter. 8 (2016) 9710–9720.
[47] X.Y. Wang, A.Q. Wang, J. Ma, J. Hazard. Mater. 336 (2017) 81–92.
[48] L. Zhao, J. Ma, Z.Z. Sun, H.L. Liu, Appl. Catal. B: Environ. 89 (2009) 326–334.
[49] J. Ding, Z. Dai, F. Qin, H.P. Zhao, S. Zhao, R. Chen, Appl. Catal. B: Environ. 205 (2017) 281–291.
[50] Y. Zheng, Z.H. Yu, F. Lin, F.S. Guo, K.A. Alamry, L.A. Taib, A.M. Asiri, X.C. Wang, Molecules 22 (2017) 572–589.
[51] L.H. Yu, X.Y. Zhang, G.W. Li, Y.T. Cao, Y. Shao, D.Z. Li, Appl. Catal. B: Environ. 187 (2016) 301–309.
[52] Y.M. Dong, H.X. Yang, K. He, X. Wu, A.M. Zhang, Appl. Catal. B: Environ. 82 (2008) 163–168.
[53] K. He, Y.M. Dong, Z. Li, L. Yin, A.M. Zhang, Y.C. Zheng, J. Hazard. Mater. 159 (2008) 587–592.
[54] Z.F. Huang, J.J. Zou, L. Pan, S.B. Wang, X.W. Zhang, L. Wang, Appl. Catal. B: Environ. 147 (2014) 167–174.
[55] H. Bader, V. Sturzenegger, J. Hoigné, Water Res. 22 (1988) 1109–1115.
[56] X.Q. Tan, Y.F. Wan, Y.J. Huang, C. He, Z.L. Zhang, Z.Y. He, L.L. Hu, J.W. Zeng, D. Shu, J. Hazard. Mater. 321 (2017) 162–172.
[57] J. Chen, D.Z. Li, J.B. Wang, P. Wang, C.S. Cao, Y. Shao, J.X. Wang, J.J. Xian, Appl. Catal. B: Environ. 163 (2015) 323–329.